Electronic Supplementary Material (ESI) for Inorganic Chemistry Frontiers.

Engineering $Cu_2O/Cu@CoO$ Hierarchical Nanospheres: Synergetic Effect of Fast Charge Transfer Cores and Active Shells for Enhanced Oxygen Evolution Reaction

Xia Zhong, Yuan Zhang, Zhibin Geng, Fangbing Shi, Mengpei Jiang, Yu Sun, Xiaofeng Wu, Keke Huang, and Shouhua Feng*

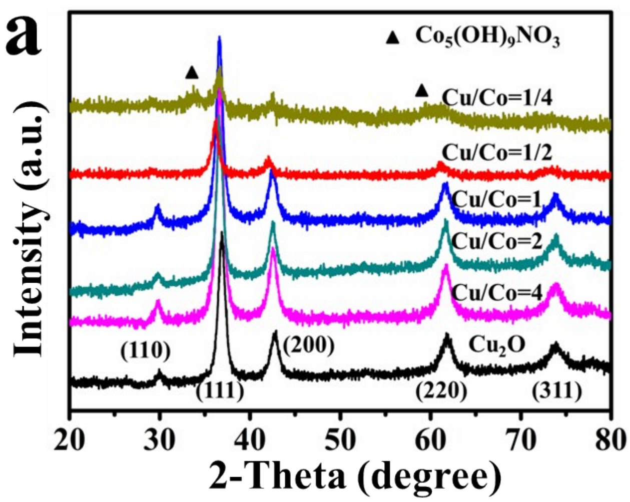

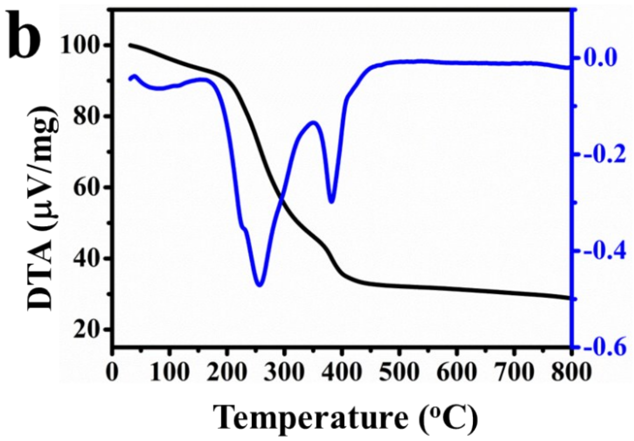

Figure S1. (a) XRD patterns of $Cu_2O@Co_5(OH)_9NO_3$ with different Cu/Co ratios; (c) TG and DTG curves for $Cu_2O@Co_5(OH)_9NO_3$ (Cu/Co= 1/2);

Fig. S1a shows the XRD patterns of the Cu_2O and $Cu_2O@Co_5(OH)_9NO_3$ core-shell samples. All of the diffraction peaks are consistent with Cu_2O (JCPDS#74-1230). Diffraction peaks of $Co_5(OH)_9NO_3$ are not obvious due to the little amount of $Co_5(OH)_9NO_3$. Until when the Cu/Co= 1/4 there appears the diffraction peaks of $Co_5(OH)_9NO_3$, which are consistent with standard PDF card of it (JCPDS#46-0605). Pure $Co_5(OH)_9NO_3$ (Fig. S3a) was synthesized by adding raw material with $Co(NO_3)_2$ only which has a hexagonal structure (JCPDS#46-0605). TG and derivative thermo gravimetric (DTG) analysis was performed to confirm the change process of $Cu_2O@Co_5(OH)_9NO_3$ (Cu/Co=1/2) annealed in tube furnace under N_2 protection. It can be seen from Fig. S1b, the precursor started to lose weight at 200 °C and a subsequent weight loss of 20% between 200 and 250 °C arose from the dehydration of $Co_5(OH)_9NO_3$ and the loss of -OH and NO_3^- corresponding to a strong exothermic peak near 250 °C in the DTA curve. There is a non-negligible mass loss about 10% in the range of 250 °C to 300 °C, which is attributed to the decomposition of Cu_2O to Cu. After elevated heating treatment, the $Cu_2O@Co_5(OH)_9NO_3$ precursor eventually transformed to Cu_2O/Cu@CoO.

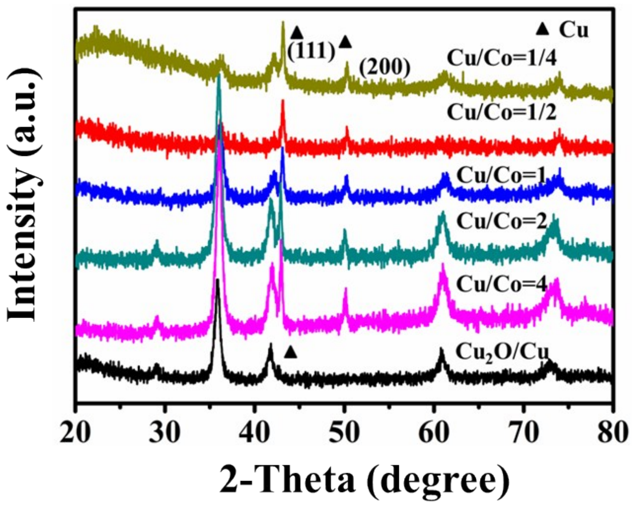

Figure S2. XRD patterns of Cu_2O/Cu@CoO with different Cu/Co ratios.

Fig. S2 shows the XRD patterns of Cu_2O/Cu and Cu_2O/Cu@CoO core-shell samples. Diffraction peak appears at 43.3° of Cu_2O/Cu is corresponding to metal Cu (JCPDS#04-0836). With the content of CoO increasing, the intensity of diffraction peaks for Cu_2O decrease and the crystallinity for core-shell composites decrease. In contrast the intensity of peaks for Cu increase which means that the content of Cu is proportional to that of CoO. Until Cu/Co= 1/2, the peak standing for Cu_2O (110) disappears completely. And Cu_2O (311) high-index facets shift to higher angle with the content of CoO increasing, which reveals the strong interactions between core and shell and provides evidence for the chemical coupling of CoO during post-thermal annealing process. The diffraction peaks of $Co_5(OH)_9NO_3$ disappear after annealing (Cu/Co= 1/4), which indicated that the decomposition of $Co_5(OH)_9NO_3$ to CoO. CoO obtained by annealed $Co_5(OH)_9NO_3$ at 300 °C under N_2 protection (Fig. S3b). The standard peaks of Cu_2O (JCPDS#74-1230) and CoO (JCPDS#43-1004) are very close. We will prove the presence of CoO in HRTEM and mapping images later.

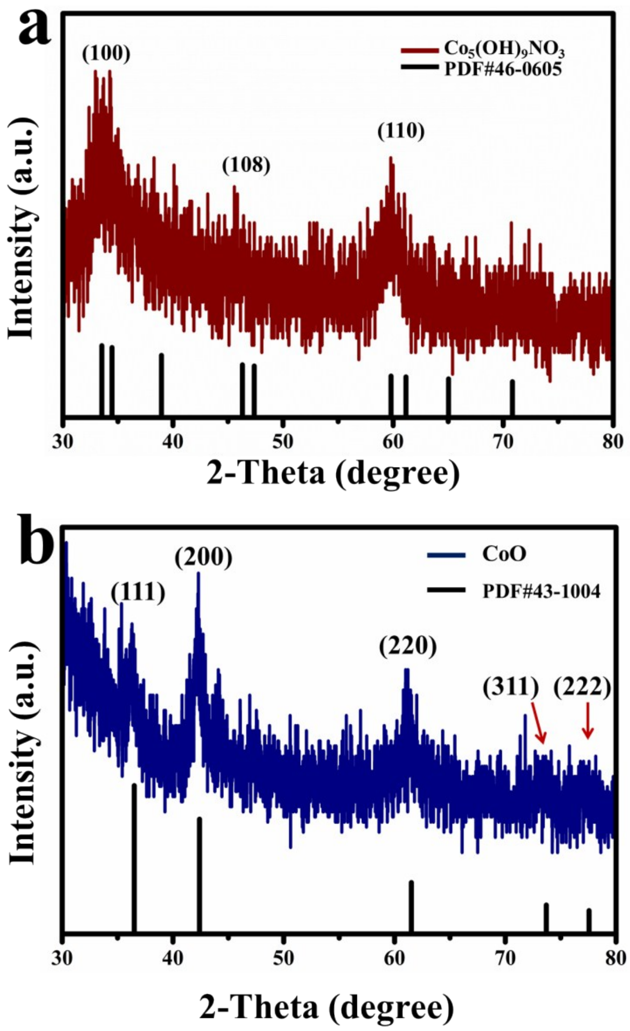

Figure S3. (a) XRD pattern of $Co_5(OH)_9NO_3$ synthesized with the same procedure as $Cu_2O@Co_5(OH)_9NO_3$ (Cu/Co= 1/2). (b) XRD pattern of CoO obtained from $Co_5(OH)_9NO_3$ annealing under N_2 at 300 ^oC for 3 h.

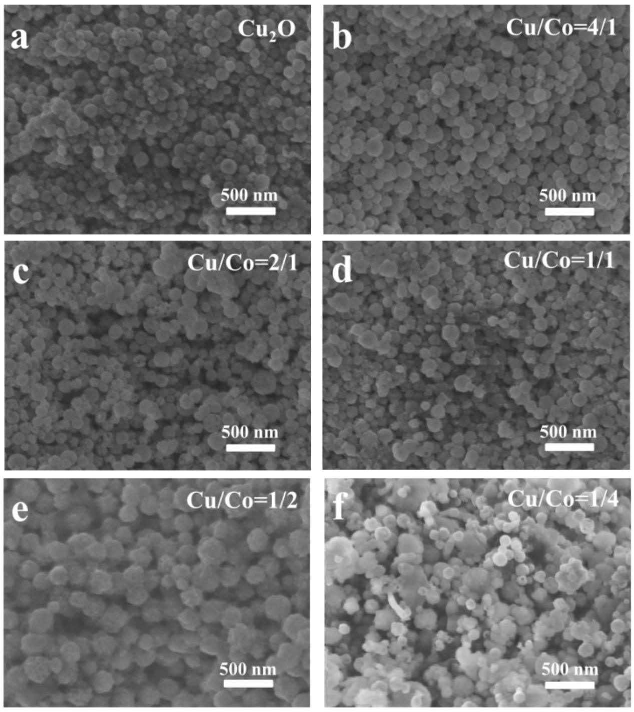

Figure S4. SEM images of $Cu_2O@Co_5(OH)_9NO_3$ with different Cu/Co ratios.

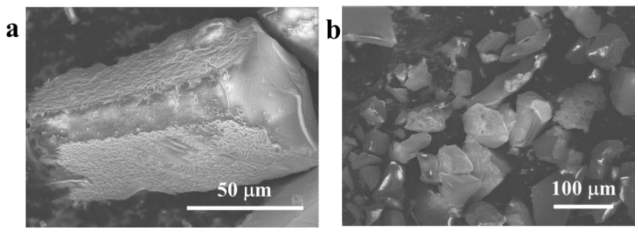

Figure S5. (a) SEM image for $Co_5(OH)_9NO_3$; (b) SEM image for CoO.

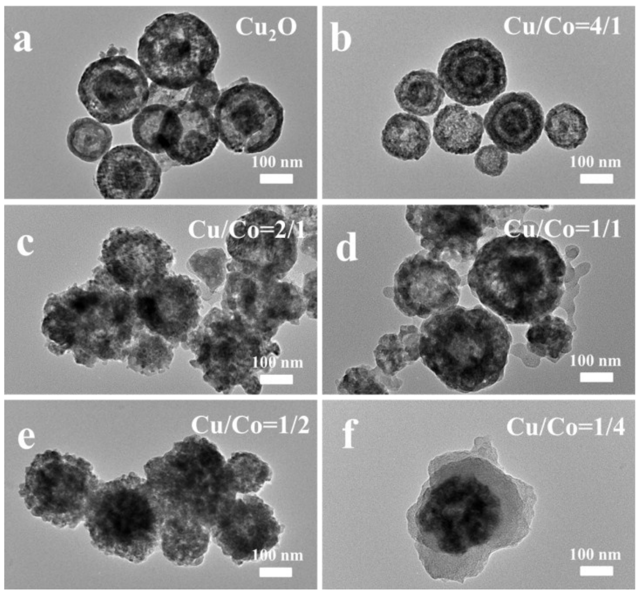

Figure S6. TEM images for Cu_2O and Cu_2O @ $Co_5(OH)_9NO_3$ with different Cu/Co ratios.

SEM (Fig. S4) was used to investigate the surface morphologies for $Cu_2O@Co_5(OH)_9NO_3$ and the inner structure was further confirmed by TEM (Fig. S4). In Fig. S4a and Fig. S6a, a cracked hollow single-shelled sphere of Cu_2O was shown. With the decrease of Cu/Co ratio (Fig. S4b-d and Fig. S6b-d), the $Co_5(OH)_9NO_3$ shell gradually appeared out of the Cu_2O cores. When the ratio coming to 1/2 (Fig. S4e and Fig. S6e), the $Co_5(OH)_9NO_3$ shell could be seen clearly uniformly distributed on the surface of Cu_2O and the addition of $Co(NO_3)_2$ makes the edge become rougher. When the ratio comes to 1/4, there are two phases in Fig. S4f, the spheres are $Cu_2O@Co_5(OH)_9NO_3$ and something that has a rod-shaped morphology are bulk $Co_5(OH)_9NO_3$ and the thickness of shell increased obviously (Fig. S6f). ($Co_5(OH)_9NO_3$ precursor has a tetragonal prism-like morphology with a micro-level size as shown in Fig. S5a.)

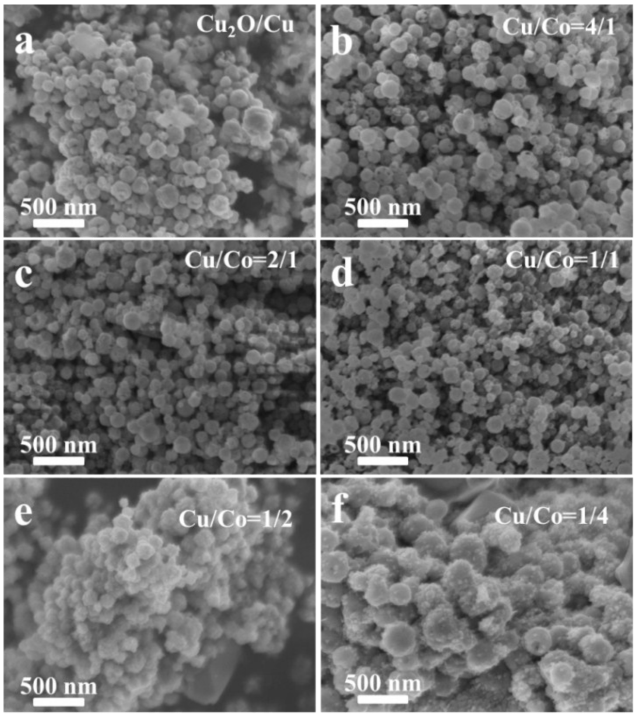

Figure S7. SEM images of Cu_2O/Cu and $Cu_2O/Cu@CoO$ with different Cu/Co ratios.

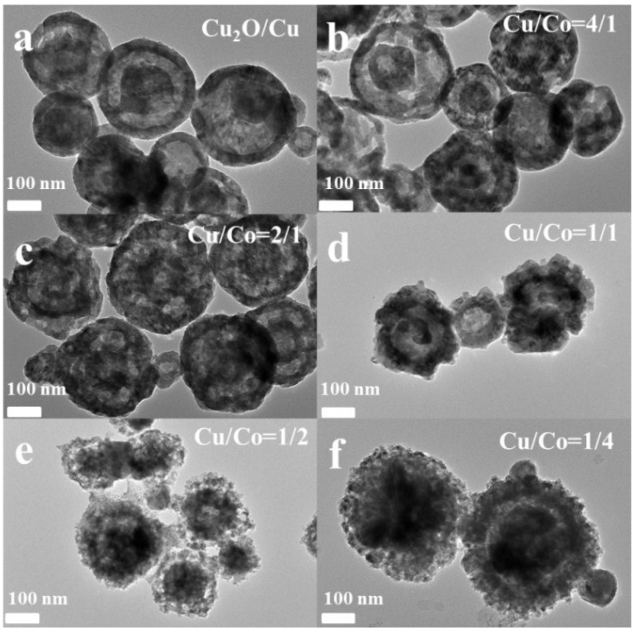

Figure S8. TEM images of Cu_2O/Cu and $Cu_2O/Cu@CoO$ with different Cu/Co ratios.

SEM images of Cu_2O/Cu and $Cu_2O/Cu@CoO$ with different Cu/Co ratios were displayed in Fig. S7. Cu_2O/Cu exhibits a hollow structure. After annealed in 300 ^oC for 3 h, the shell of $Cu_2O@Co_5(OH)_9NO_3$ decomposed to small CoO particles, coating on the surface of Cu_2O/Cu. When the Cu/Co= 4/1, hollow Cu_2O/Cu core still can be observed. With the Cu/Co ratio decrease, the CoO shell gradually appeared out of the Cu_2O/Cu core. When Cu/Co= 1/4, the CoO nanoparticles can be seen coating on the Cu_2O/Cu core clearly. (CoO has a tetragonal prism-like morphology with a micro-level size has shown in Fig. S5b.) The TEM images of Cu_2O/Cu and $Cu_2O/Cu@CoO$ were displayed in Fig. S8. Cu_2O/Cu spheres with clear hollow structure were shown in Fig. S8a. With the decrease of Cu/Co ratio, there appears thin layer CoO coupling on the surface of Cu_2O/Cu core. When the ratio comes to 1/1, there are obvious CoO shells covered on the hollow Cu_2O/Cu cores. With the Cu/Co ratio decrease to 1/2, CoO shell with an average thickness of 10 nm was uniformly distributed on the surface of hollow Cu_2O/Cu core. When the Cu/Co= 1/4, the thickness of shell increased to 20 nm. The sizes of $Cu_2O/Cu@CoO$ with different Cu/Co ratios almost keep at an average diameter of 150 nm uniformly but the cores of $Cu_2O/Cu@CoO$ (Cu/Co= 1, 1/2/, 1/4) has slightly collapsed since parts of Cu_2O decomposed to Cu.

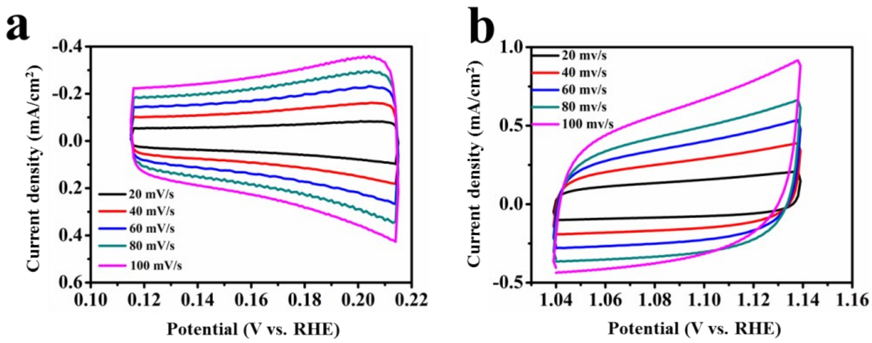

Figure S9. Cyclic voltammograms of Cu_2O (a) and Cu_2O/Cu (b).

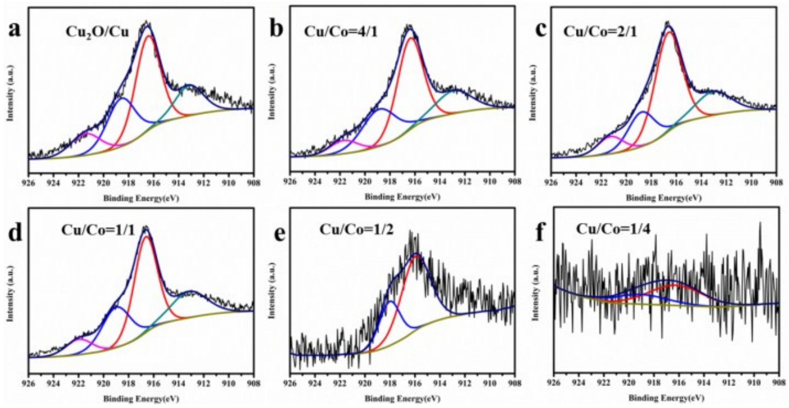

Figure S10. Cu *LMM* Auger spectra of Cu_2O/Cu and $Cu_2O/Cu@CoO$ with different Cu/Co ratios.

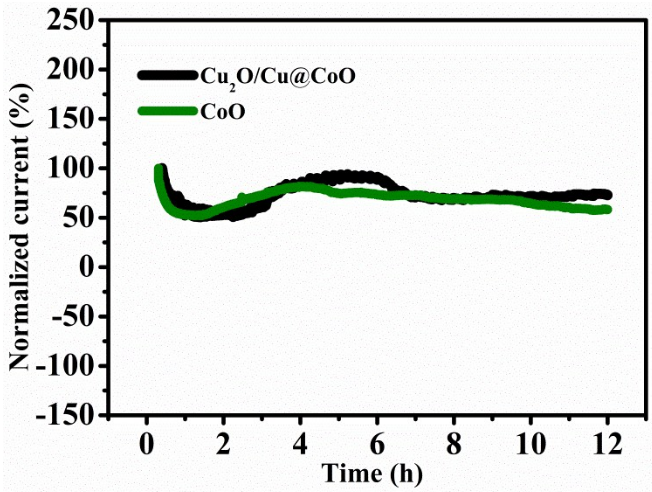

Figure S11. Chronoamperometric curves obtained for $Cu_2O/Cu@CoO$ and CoO at a potential of 1.6 V vs RHE.

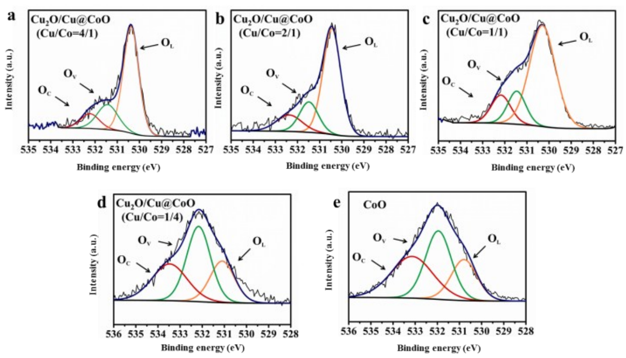

Figure S12. XPS spectrum of O 1s in $Cu_2O/Cu@CoO$ with different Cu/Co ratios and CoO.

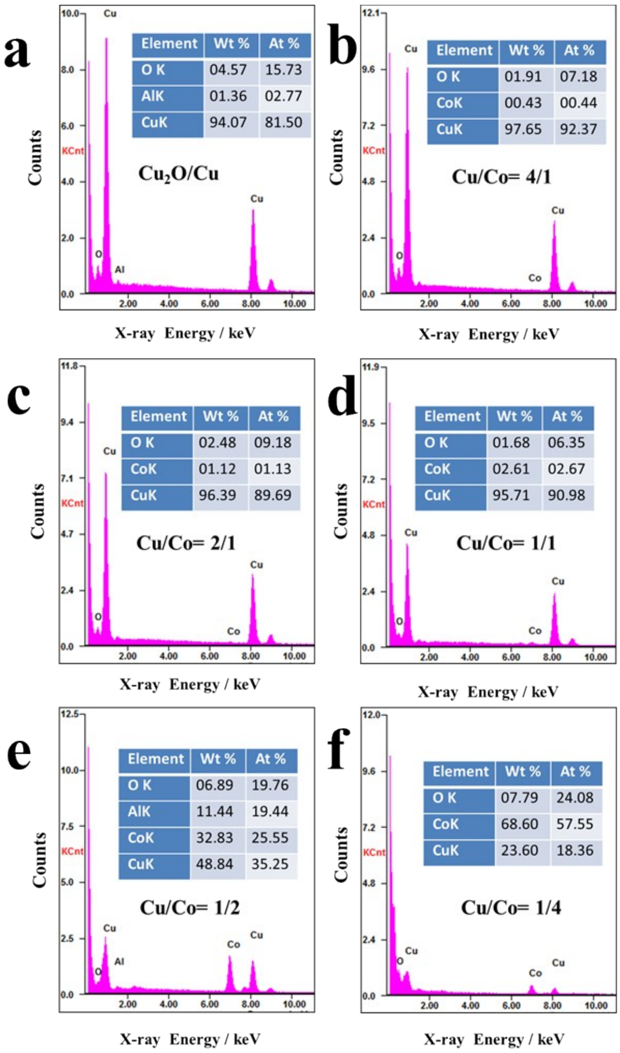

Figure S13. EDS results of Cu_2O/Cu and Cu_2O/Cu@CoO with different Cu/Co ratios.